This paper is published as part of a PCCP Themed Issue on:

Physical chemistry of solids – the science behind materials engineering

Guest Editors: Jürgen Janek, Manfred Martin and Klaus Dieter Becker

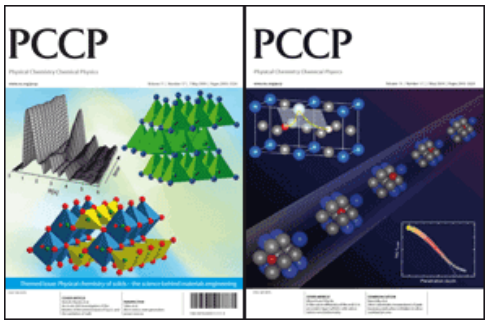

Editorial

Physical chemistry of solids—the science behind materials engineering
Phys. Chem. Chem. Phys., 2009
DOI: 10.1039/b905911n

Perspectives

Nanoionics: ionic charge carriers in small systems
Joachim Maier, *Phys. Chem. Chem. Phys.*, 2009
DOI: 10.1039/b902586n

Micro-ionics: next generation power sources
Harry L. Tuller, Scott J. Litzelman and WooChul Jung, *Phys. Chem. Chem. Phys.*, 2009
DOI: 10.1039/b901906e

Communications

On the conduction pathway for protons in nanocrystalline yttria-stabilized zirconia
Sangtae Kim, Hugo J. Avila-Paredes, Shizhong Wang, Chien-Ting Chen, Roger A. De Souza, Manfred Martin and Zuhair A. Munir, *Phys. Chem. Chem. Phys.*, 2009
DOI: 10.1039/b901623f

Direct calorimetric measurement of grain boundary and surface enthalpies in yttria-stabilized zirconia
Shushu Chen, Hugo J. Avila-Paredes, Sangtae Kim, Jinfeng Zhao, Zuhair A. Munir and Alexandra Navrotsky, *Phys. Chem. Chem. Phys.*, 2009
DOI: 10.1039/b819740g

Papers

Elastic strain at interfaces and its influence on ionic conductivity in nanoscaled solid electrolyte thin films—theoretical considerations and experimental studies
N. Schichtel, C. Korte, D. Hesse and J. Janek, *Phys. Chem. Chem. Phys.*, 2009
DOI: 10.1039/b900148d

Chemical and electronic properties of the ITO/Al_2O_3 interface
Yvonne Gassenbauer, André Wachau and Andreas Klein, *Phys. Chem. Chem. Phys.*, 2009
DOI: 10.1039/b822848e

Electronic state of oxygen nonstoichiometric $La_{2-x}Sr_xNiO_{4+\delta}$ at high temperatures
Takashi Nakamura, Keiji Yashiro, Kazuhisa Sato and Junichiro Mizusaki, *Phys. Chem. Chem. Phys.*, 2009
DOI: 10.1039/b823364k

B-Site cation diffusivity of Mn and Cr in perovskite-type $LaMnO_3$ with cation-deficit nonstoichiometry
Shogo Miyoshi and Manfred Martin, *Phys. Chem. Chem. Phys.*, 2009
DOI: 10.1039/b901208g

High anion conductivity in a ternary non-equilibrium phase of BaF_2 and CaF_2 with mixed cations
B. Ruprecht, M. Wilkening, A. Feldhoff, S. Steuernagel and P. Heitjans, *Phys. Chem. Chem. Phys.*, 2009
DOI: 10.1039/b901293a

Electrical and optical characterization of undoped $BaTiO_3$ in the quenched state
K.-D. Becker, M. Schrader, H.-S. Kwon and H.-I. Yoo, *Phys. Chem. Chem. Phys.*, 2009
DOI: 10.1039/b823174e

Oxidation states of Co and Fe in $Ba_{1-x}Sr_xCo_{1-y}Fe_yO_{3-\delta}$ (x, y = 0.2–0.8) and oxygen desorption in the temperature range 300–1273 K
Ashley S. Harvey, F. Jochen Litterst, Zhen Yang, Jennifer L. M. Rupp, Anna Infortuna and Ludwig J. Gauckler, *Phys. Chem. Chem. Phys.*, 2009
DOI: 10.1039/b819414a

Bulk defect chemistry and surface electronic behavior of Zn,Sn codoped In_2O_3 transparent conducting oxides
Steven P. Harvey, Thomas O. Mason, Christoph Körber and Andreas Klein, *Phys. Chem. Chem. Phys.*, 2009
DOI: 10.1039/b822149a

Defect chemistry of the cage compound, $Ca_{12}Al_{14}O_{33-\delta}$—understanding the route from a solid electrolyte to a semiconductor and electride
Doh-Kwon Lee, Lutz Kogel, Stefan G. Ebbinghaus, Ilia Valov, Hans-Dieter Wiemhoefer, Martin Lerch and Juergen Janek, *Phys. Chem. Chem. Phys.*, 2009
DOI: 10.1039/b818474g

Electrical conductivity–defect structure correlation of variable-valence and fixed-valence acceptor-doped $BaTiO_3$ in quenched state
Han-Ill Yoo, Tae-Sik Oh, Hyung-Soon Kwon, Dong-Kyu Shin and Jong-Sook Lee, *Phys. Chem. Chem. Phys.*, 2009
DOI: 10.1039/b822381p

An *in situ* XAS investigation of the kinetics of the ammonolysis of Ga_2O_3 and the oxidation of GaN
J. Brendt, D. Samuelis, T. E. Weirich and M. Martin, *Phys. Chem. Chem. Phys.*, 2009
DOI: 10.1039/b901819k

***In situ* investigation of coloration processes in $LiNbO_3$: MgO during reducing/oxidizing high-temperature treatments**
Dmytro Sugak, Yaroslav Zhydachevskii, Yuriy Sugak, Oleg Buryy, Sergii Ubizskii, Ivan Solskii, Alexander Börger and Klaus-Dieter Becker, *Phys. Chem. Chem. Phys.*, 2009
DOI: 10.1039/b822631h

Voltage-assisted ^{18}O tracer incorporation into oxides for obtaining shallow diffusion profiles and for measuring ionic transference numbers: basic considerations
J. Fleig, *Phys. Chem. Chem. Phys.*, 2009
DOI: 10.1039/b822415c

Oxygen incorporation into strontium titanate single crystals from CO_2 dissociation
Chr. Argirusis, F. Voigts, P. Datta, J. Grosse-Brauckmann and W. Maus-Friedrichs, *Phys. Chem. Chem. Phys.*, 2009
DOI: 10.1039/b901401b

Nearly constant loss effects in borate glasses
David M. Laughman, Radha D. Banhatti and Klaus Funke, *Phys. Chem. Chem. Phys.*, 2009
DOI: 10.1039/b822561n**Switching behaviour of modulated ferroelectrics I: kinetics of the field-induced lock-in transition of Rb_2ZnCl_4**
K. Elisbihani, H. Gibhardt and G. Eckold, *Phys. Chem. Chem. Phys.*, 2009
DOI: 10.1039/b902368b

Construction of nano- and microporous frameworks from octahedral bubble clusters
S. M. Woodley, M. B. Watkins, A. A. Sokol, S. A. Shevlin and C. R. A. Catlow, *Phys. Chem. Chem. Phys.*, 2009
DOI: 10.1039/b902600b

Bubbles and microporous frameworks of silicon carbide
M. B. Watkins, S. A. Shevlin, A. A. Sokol, B. Slater, C. R. A. Catlow and S. M. Woodley, *Phys. Chem. Chem. Phys.*, 2009
DOI: 10.1039/b902603g

Band gap engineering of ZnO *via* doping with manganese: effect of Mn clustering
Hilkka Saal, Thomas Bredow and Michael Binnewies, *Phys. Chem. Chem. Phys.*, 2009
DOI: 10.1039/b901596e

Transport pathways for mobile ions in disordered solids from the analysis of energy-scaled bond-valence mismatch landscapes
Stefan Adams and R. Prasada Rao, *Phys. Chem. Chem. Phys.*, 2009
DOI: 10.1039/b901753d

Ultrathin oxide films and heterojunctions: CaO layers on BaO and SrO
Chris E. Mohn, Neil L. Allan and John H. Harding, *Phys. Chem. Chem. Phys.*, 2009
DOI: 10.1039/b822588e

Formation entropies of intrinsic point defects in cubic In_2O_3 from first-principles density functional theory calculations
Péter Ágoston and Karsten Albe, *Phys. Chem. Chem. Phys.*, 2009
DOI: 10.1039/b900280d

Hydrogen adsorption on Pd-containing Au(111) bimetallic surfaces
Sudha Venkatachalam and Timo Jacob, *Phys. Chem. Chem. Phys.*, 2009
DOI: 10.1039/b900250b

Interdiffusion and surface-sandwich ordering in initial Ni-core–Pd-shell nanoparticle
Alexander V. Evteev, Elena V. Levchenko, Irina V. Belova and Graeme E. Murch, *Phys. Chem. Chem. Phys.*, 2009
DOI: 10.1039/b822112j

First-principles study on defect chemistry and migration of oxide ions in ceria doped with rare-earth cations
Masanobu Nakayama and Manfred Martin, *Phys. Chem. Chem. Phys.*, 2009
DOI: 10.1039/b900162j**An electrochemical study of lithium insertion into $Cr_{5-y}Ti_ySe_8$ (y = 1, 2, 3, 4, 4.5) beyond the intercalation limit**
Sylvio Indris, Joseph Wontcheu and Wolfgang Bensch, *Phys. Chem. Chem. Phys.*, 2009
DOI: 10.1039/b822397a

Mixed $LiCo_{0.6}M_{0.4}PO_4$ (M = Mn, Fe, Ni) phosphates: cycling mechanism and thermal stability
Natalia N. Bramnik, Dmytro M. Trots, Heiko J. Hofmann and Helmut Ehrenberg, *Phys. Chem. Chem. Phys.*, 2009
DOI: 10.1039/b901319a

Changes in the crystal and electronic structure of $LiCoO_2$ and $LiNiO_2$ upon Li intercalation and de-intercalation
Sonja Laubach, Stefan Laubach, Peter C. Schmidt, David Ensling, Stefan Schmid, Wolfram Jaegermann, Andreas Thißen, Kristian Nikolowski and Helmut Ehrenberg, *Phys. Chem. Chem. Phys.*, 2009
DOI: 10.1039/b901200a

Partial oxidation of methanol on well-ordered V_2O_5(001)/Au(111) thin films
J. M. Sturm, D. Göbke, H. Kuhlenbeck, J. Döbler, U. Reinhardt, M. V. Ganduglia-Pirovano, J. Sauer and H.-J. Freund, *Phys. Chem. Chem. Phys.*, 2009
DOI: 10.1039/b822384j

Investigation of the nucleation and growth dynamics of FePt nanoparticles prepared *via* a high-temperature synthesis route employing $PtCl_2$ as platinum precursor
Hauke Heller, Kirsten Ahrenstorf, Jose A. C. Broekaert and Horst Weller, *Phys. Chem. Chem. Phys.*, 2009
DOI: 10.1039/b822306h

Non-oxidic nanoscale composites: single-crystalline titanium carbide nanocubes in hierarchical porous carbon monoliths
Kirstin Sonnenburg, Bernd M. Smarsly and Torsten Brezesinski, *Phys. Chem. Chem. Phys.*, 2009
DOI: 10.1039/b822437d

Poly(p-phenylene sulfone)s with high ion exchange capacity: ionomers with unique microstructural and transport features
C. C. de Araujo, K. D. Kreuer, M. Schuster, G. Portale, H. Mendil-Jakani, G. Gebel and J. Maier, *Phys. Chem. Chem. Phys.*, 2009
DOI: 10.1039/b822069g

Pulsed electrodeposition of porous ZnO on Ag-coated polyamide filaments
Melanie Rudolph, Thomas Loewenstein, Elisa Arndt, Yvonne Zimmermann, Andreas Neudeck and Derck Schlettwein, *Phys. Chem. Chem. Phys.*, 2009
DOI: 10.1039/b822534f

Mixed $LiCo_{0.6}M_{0.4}PO_4$ (M = Mn, Fe, Ni) phosphates: cycling mechanism and thermal stability

Natalia N. Bramnik,*[ab] Dmytro M. Trots,[c] Heiko J. Hofmann[a] and Helmut Ehrenberg[b]

Received 21st January 2009, Accepted 11th February 2009
First published as an Advance Article on the web 9th March 2009
DOI: 10.1039/b901319a

The electrochemical delithiation of $LiCo_{0.6}M_{0.4}PO_4$ phosphates (M = Mn, Fe, Ni) was studied by *in situ* synchrotron diffraction. In all three metallophosphates the oxidation–reduction of 3d-elements proceed *via* two-phase mechanisms leading to two-phase regions, corresponding to the Co^{2+}/Co^{3+} and M^{2+}/M^{3+} reactions. The Ni^{2+}/Ni^{3+} reaction was not revealed, neither by the potentiostatic intermittent titration technique (PITT) nor by diffraction. In the two-phase reaction, the olivine-like structure of the cathode remains preserved, which is characteristic of this type of materials. Pronounced solid-solution domains were observed during both lithium extraction and insertion. The thermal stability of the charged cathodes is limited by the presence of Co^{3+} and its intrinsic instability in these compounds.

Introduction

The electrochemical activity of $LiMPO_4$ cathode materials (M = Mn, Fe, Co, Ni) can be significantly influenced by the combination of two or more electrochemically active 3d elements in the lattice. The most known example is the enhanced kinetics of Mn^{3+}/Mn^{2+} couple if Mn and Fe share the octahedral site in the olivine-like structure $LiMn_yFe_{1-y}PO_4$.[1–3] In the pure $LiMnPO_4$, several factors were argued to be responsible for the extremely low rate capability of this material, including large effective mass of polarons around Jahn–Teller active Mn^{3+} in $MnPO_4$ together with strong local lattice deformation.[2,4] The incorporation of Fe on the Mn site was shown to reduce the degree of distortion of $M^{3+}O_6$ octahedra in $Mn_yFe_{1-y}PO_4$ ($y < 0.8$) in comparison with $MnPO_4$ and, thus, may stabilize the lattice of the delithiated compound against the strain.[3] Nevertheless, the positive influence of Fe-substitution on the kinetics of Li-extraction in these systems is still not well understood.

In addition to the kinetic aspect, the coexistence of two electrochemically active elements may impact the character of the delithiation mechanism. The structural changes upon delithiation of $LiMn_yFe_{1-y}PO_4$ were extensively studied by Yamada *et al.*[2,3,5] When Mn and Fe are randomly distributed on the octahedral 4c site, the Fe^{2+}/Fe^{3+} reaction was shown to proceed (partially or entirely) *via* a solid solution mechanism.[5] In later works, Molenda *et al.* observed a single phase mechanism in the whole range of the lithium content for the stoichiometry $Li_yFe_{0.45}Mn_{0.55}PO_4$ (y = 1.0–0.16).[6,7] It implies a single phase mechanism also for the Mn^{2+}/Mn^{3+} reaction, which disagrees with the data reported by Bramnik *et al.*[8] and Burba *et al.*[9] for similar compositions. The mixed Mn–Fe phosphates are promising cathode materials due to low cost, stable cycling behaviour and good rate capability.[10,11]

The combination of Fe and Co in the crystal structure of olivine-like metallophosphates was also explored by several groups.[12–17] At high cobalt contents, the operation in the voltage range corresponding to the Co^{3+}/Co^{2+} electrochemical reaction (4.8 V *vs.* Li/Li^+) is accompanied by the fast capacity fading of the cell, which was ascribed to the oxidative electrolyte degradation.[12] The problem of the anodic stability of the electrolyte should be even more serious for $LiNi_yCo_{1-y}PO_4$ cathode materials,[18,19] because of the higher oxidation potential of Ni^{3+}/Ni^{2+} (>5 V *vs.* Li/Li^+).[20]

Recently, we reported on synchrotron and neutron diffraction studies of $LiCoPO_4$ delithiation.[21,22] The two olivine-like phases, which appear during charging of a cell with a $LiCoPO_4$-based cathode, Li_zCoPO_4 (z = 0.6) and $CoPO_4$, were shown to be thermally unstable and decompose at moderate heating (>100 °C) in inert atmosphere.[23] Here, we applied *in situ* synchrotron diffraction to reveal the structural changes during delithiation of $LiCo_{0.6}M_{0.4}PO_4$ (M = Mn, Fe, Ni). Additionally, the thermal stability of the charged cathodes is discussed.

Experimental

$LiCo_{0.6}M_{0.4}PO_4$ (M = Fe, Mn, Ni) materials were prepared by a solid-state reaction of Li_2CO_3 (Aldrich, 99%), $(NH_4)_2HPO_4$ (Aldrich, 99.8%) and an appropriate salt ($FeC_2O_4{\cdot}2H_2O$ (99%, Aldrich), $Mn(CH_3COO)_2{\cdot}4H_2O$, $Co(CH_3COO)_2{\cdot}4H_2O$ or $Ni(CH_3COO)_2{\cdot}4H_2O$, respectively, all ≥ 99.0% purchased from Fluka). The components were ground with acetone in an agate mortar, pressed as a pellet and pre-annealed at 400 °C for 3 h. After re-grounding and pressing, the pellets were annealed at 600 °C for 12 h. All

[a] *Institute for Materials Science, University of Technology, Petersenstr. 23, 64287 Darmstadt, Germany. E-mail: bramnik@tu-darmstadt.de; Fax: +49 (0)6151 166023; Tel: +49 (0)6151 166359*
[b] *Institute for Complex Materials, IFW Dresden, Helmholtzstr. 20, 01069 Dresden, Germany*
[c] *HASYLAB/DESY, Notkestr. 85, 22607 Hamburg, Germany*

thermal treatments for $LiCo_{0.6}Fe_{0.4}PO_4$ were performed under argon flow.

To prepare the electrode, the metallophosphate (75% w/w) was mixed with acetylene carbon black (20% w/w) and PVdF (5%), pressed on the Al-mesh (for PITT experiments) or as a pellet (for *in situ* synchrotron diffraction) and dried in vacuum at 100 °C. The electrochemical cells consist of Li as the negative electrode, a glass-fiber separator and 1 M $LiPF_6$ in EC-DMC (1 : 2) as electrolyte (Ferro, USA) and were assembled in an argon-filled glove box. The cell design used for *in situ* diffraction was published earlier.[24] All electrochemical measurements were carried out with a potentiostat VMP (Perkin-Elmer Instruments, USA).

In situ synchrotron diffraction was performed at the powder diffractometer B2 (HASYLAB/DESY, Hamburg, Germany).[25] The diffraction patterns were collected with an on-site readable image plate detector.[26] The wavelength $\lambda = 0.49324$ Å was selected with a Si(111) double-crystal monochromator. Rietveld analyses, based on the synchrotron data, were performed with the software package Fullprof.

Thermal analysis of the charged cathodes was performed with a Netzsch STA 429 device at a heating rate of 2 K min^{-1} in argon.

Results and discussions

The oxidation–reduction steps in the mixed $LiCo_{0.6}M_{0.4}PO_4$ (M = Mn, Fe, Ni) phosphates can be clearly distinguished in the incremental capacity plot (Fig. 1). In accordance with previous reports, the coexistence of two 3d-elements on the octahedral sites of the olivine-like structure does not result in a significant change of the thermodynamic potentials of the individual couples M^{3+}/M^{2+}. The oxidation-reduction of Fe (3.4–3.5 V *vs.* Li/Li^+) and Mn (4.0–4.5 V *vs.* Li/Li^+) occurs at voltages lower than the potential of the Co^{3+}/Co^{2+} couple and, therefore, at the potentials, which were reported for the oxidation–reduction of $LiFePO_4$ and $LiMnPO_4$, respectively. The electrochemical activity of the Ni^{2+}/Ni^{3+} couple in $LiCo_{0.6}Ni_{0.4}PO_4$ is questionable. According to ref. 18 the redox potential of Ni in $LiNiPO_4$ is between 5.1 and 5.3 V. Under the conditions of our PITT experiment, we observed no electrochemical activity at potentials between 5 and 5.2 V *vs.* Li/Li^+ (see Fig. 1c). The amount of extracted Li in the PITT experiment corresponds also to the oxidation of Co in $LiCo_{0.6}Ni_{0.4}PO_4$ only.

The maxima of the oxidation peaks, corresponding to the Co^{2+}/Co^{3+} reactions, are located at 4.8 V *vs.* Li/Li^+ for all three phosphates, shown in Fig. 1. This value is very close to the oxidation potentials 4.79 and 4.87 V *vs.* Li/Li^+, previously reported for the two-step oxidation Co^{2+}/Co^{3+} in pure $LiCoPO_4$.[21] In contrast to the latter, in the mixed phosphates with composition $LiCo_{0.6}M_{0.4}PO_4$ (M = Mn, Fe, Ni), the redox behaviour of Co seems to be reflected by one oxidation and one reduction peak only. At the same time, the "Co-peaks" are accompanied by shoulders in all three mixed phosphates. These shoulders correspond to the voltage regions, where one electrochemical reaction is replaced by another one (left from Co-peak for $LiCo_{0.6}Fe_{0.4}PO_4$ and $LiCo_{0.6}Mn_{0.4}PO_4$ and right for $LiCo_{0.6}Ni_{0.4}PO_4$, respectively).

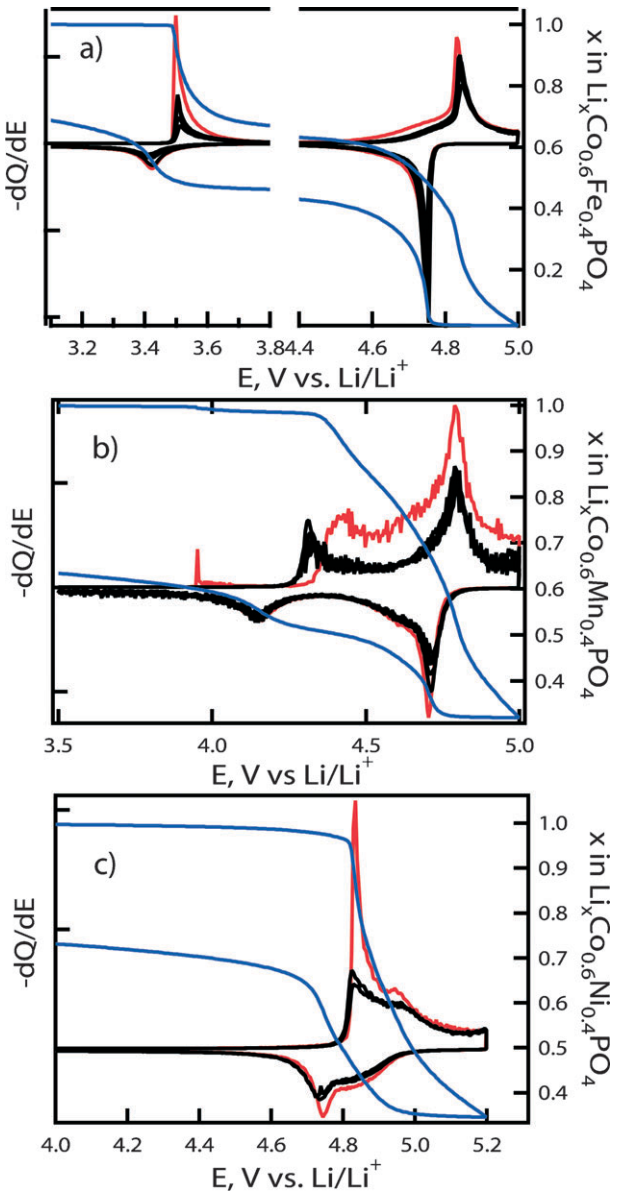

Fig. 1 Incremental capacity plot for (a) $LiCo_{0.6}Fe_{0.4}PO_4$, (b) $LiCo_{0.6}Mn_{0.4}PO_4$ and (c) $LiCo_{0.6}Ni_{0.4}PO_4$ (I_{lim} is close to C/12). The First cycle is shown as red. The blue line shows the change of the Li-content in the cathode during the first cycle (right axis).

It can indicate the solid-solution domains in the extraction–insertion mechanism, which will be discussed later in details.

During the *in situ* synchrotron diffraction experiments, the electrochemical cells were charged galvanostatically to composition $Li_xCo_{0.6}M_{0.4}PO_4$, $x \approx 0$. As previously demonstrated for $LiCoPO_4$,[21] the Li contents calculated from the flown charge should be considered with care, because parasitic electrochemical reactions can bias the nominal Li-content, especially in the high-voltage region. Any contribution from parasitic reactions to the overall current results in an overestimation of the lithium extraction. For all three compounds, not more than 0.6 Li per formula unit can be re-inserted in the cathode upon discharge in the *in situ* experiment. It is a further indication of an actual lower degree of charge in the *in situ* experiment than the 100% determined from the extracted/inserted charge.

Selected regions in the synchrotron diffraction patterns, representing the evolution of the cathode structure, are shown in Fig. 2–4 for all three metallophosphates. Rietveld analysis reveals that the olivine-like structure of the cathode materials remains preserved for all phases appearing during the operation of the cells. To reveal the unit cell parameters and phase ratios at different stages of charge, Rietveld refinements were performed for all delithiated phases with initial models based on the structures of the pristine compounds (S.G. *Pnma*) without cation/anion deficiency nor M1(Li-sites)/M2(Co/M-sites) disorder. For all data sets, scale factors, cell parameters, background and profile parameters were refined. The evolutions of the cell parameters are summarized in Fig. 5–8.

$LiCo_{0.6}Fe_{0.4}PO_4$

The extraction of Li from $LiCo_{0.6}Fe_{0.4}PO_4$ occurs *via* two successive two-phase regions, which are separated by a solid-solution domain (Fig. 5). We disregard the short range in the

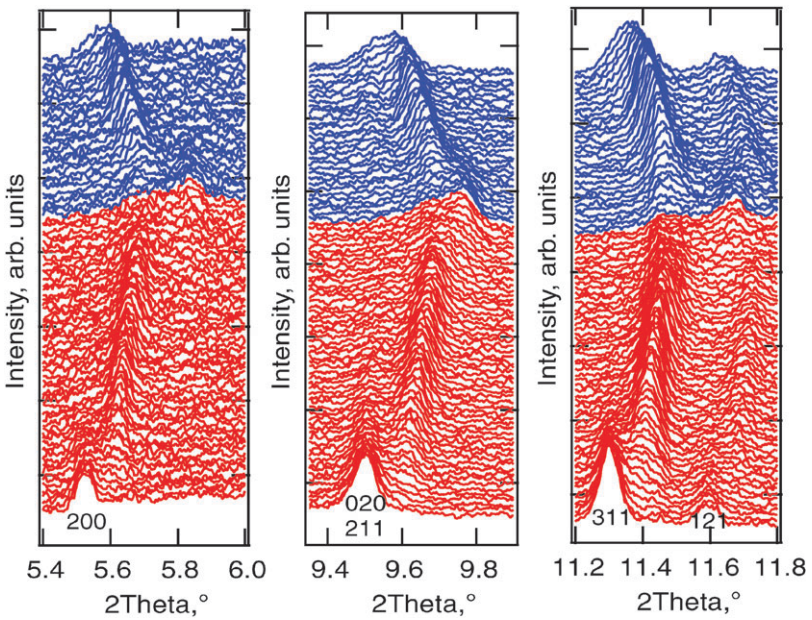

Fig. 2 Selected regions in the synchrotron diffraction patterns for $LiCo_{0.6}Fe_{0.4}PO_4$ measured during the first cycle (C/14) of the *in situ* electrochemical cell (red: charge to the concentration $x = 0$ in $Li_xCo_{0.6}Fe_{0.4}PO_4$ (5.0 V *vs.* Li/Li^+), blue: discharge to the concentration x = 0.54 (2.5 V *vs.* Li/Li^+) as calculated from the electrochemical data).

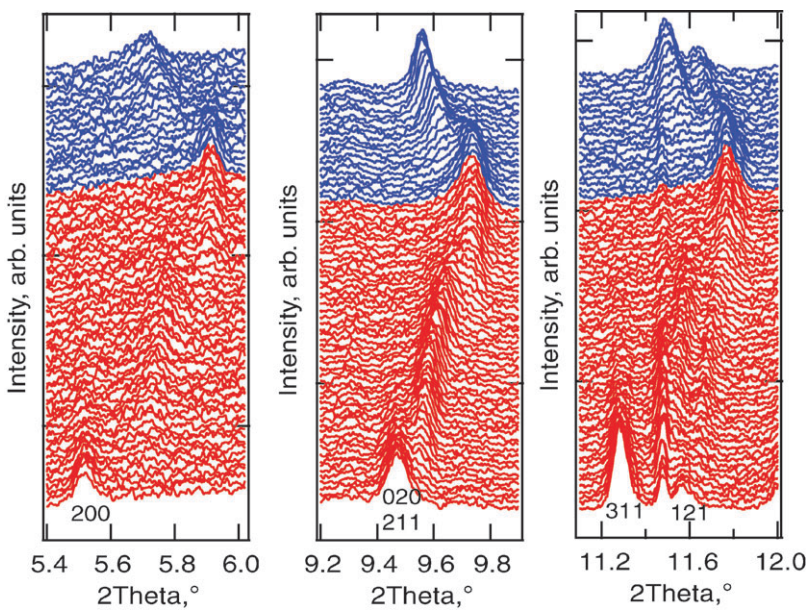

Fig. 3 Selected regions in the synchrotron diffraction patterns for $LiCo_{0.6}Mn_{0.4}PO_4$ measured during the first cycle (C/14) of the *in situ* electrochemical cell (red: charge to the concentration $x = 0$ in $Li_xCo_{0.6}Mn_{0.4}PO_4$ (5.05 V *vs.* Li/Li^+), blue: discharge to the concentration $x = 0.4$ (2.5 V *vs.* Li/Li^+) as calculated from the electrochemical data).

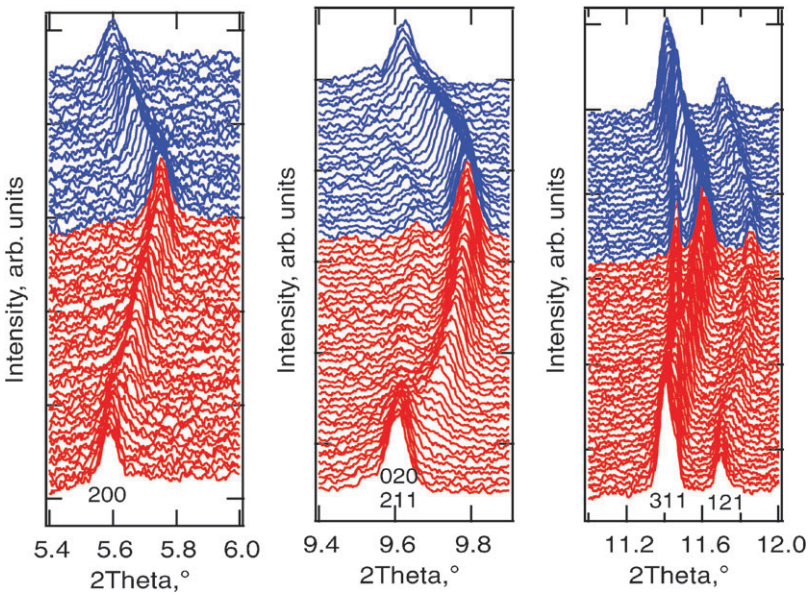

Fig. 4 Selected regions in the synchrotron diffraction patterns for $LiCo_{0.6}Ni_{0.4}PO_4$ measured during the first cycle (C/11) of the *in situ* electrochemical cell (red: charge to the concentration $x = 0$ in $Li_xCo_{0.6}Ni_{0.4}PO_4$ (5.25 V *vs.* Li/Li^+), blue: discharge to the concentration $x = 0.51$ (3.1 V *vs.* Li/Li^+) as calculated from the electrochemical data).

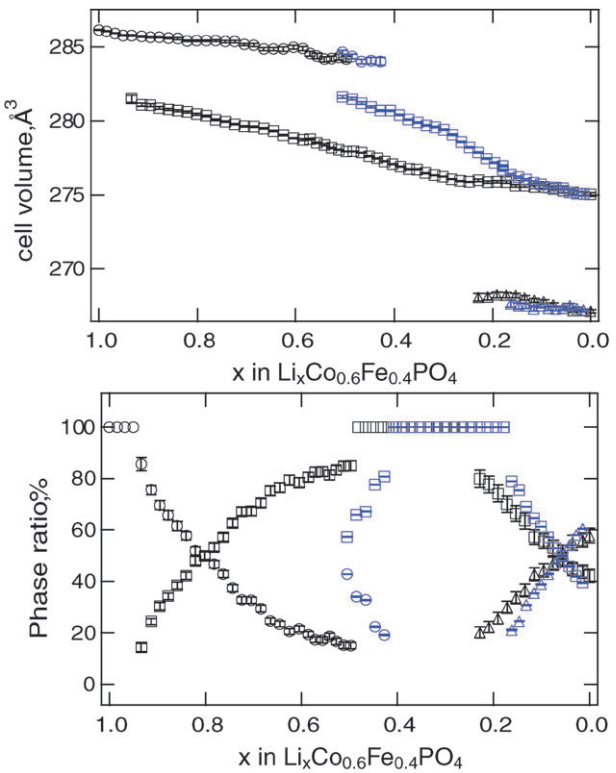

Fig. 5 Unit cell volumes and phase ratios evolution during galvanostatic (C/14) charge-discharge of $LiCo_{0.6}Fe_{0.4}PO_4$-cell. Black symbols represent charge, blue: discharge processes. The parameters of pristine phase are shown with cycles. Squares indicate the phase appearing in the middle of charge-discharge as well as solid-solition regions. The phase appearing at high degree of delithiation is marked with triangles.

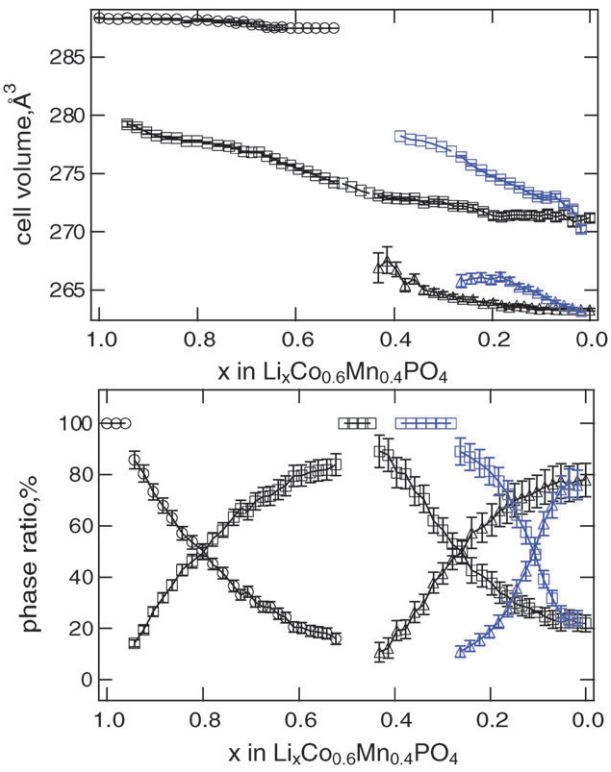

Fig. 6 Same as Fig. 5, but for $LiCo_{0.6}Mn_{0.4}PO_4$-cell.

beginning of charge ($0.92 < x < 1$), where a single olivine-phase model was also applied. One can speculate, that the mixed phosphates studied here have a narrow "miscibility gap" at the beginning of delithiation as extensively discussed for $LiFePO_4$.[27,28] On the other hand, such a solid-solution region at the beginning of delithiation was shown to be most pronounced for nanoscale $LiFePO_4$ and completely disappears for particle sizes >100 nm.[27] We believe that a two-phase mechanism at the beginning of the $LiCo_{0.6}Fe_{0.4}PO_4$ delithiation is favoured over a "solid-solution" one, but cannot be

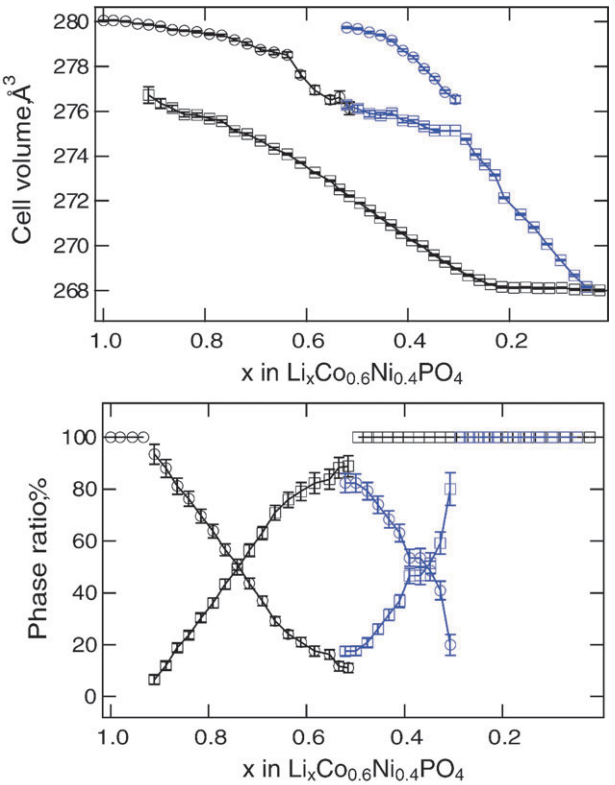

Fig. 7 Same as Fig. 5, but for $LiCo_{0.6}Ni_{0.4}PO_4$-cell and for different charge–discharge rate (C/11).

determined unambiguously because of the low amount of the second phase, close or below the detection limit. For the other metallophosphates, very similar regions are observed at the initial stages of lithium extraction (see Fig. 6 and 7).

The first phase transition (extraction of ~50% Li) corresponds to the oxidation of Fe. This region is slightly broader than that expected from the stoichiometry of the pristine compound, implying that the oxidation of Fe is already complete by the extraction of 40% Li. Note that the determination of the borderline between the two-phase region and the subsequent solid-solution domain is not unambiguous, because the amount of the pristine compound is very low and does not change significantly in the range $0.5 < x < 0.7$ in $Li_xCo_{0.6}Fe_{0.4}PO_4$. In this region, the volume of the delithiated phase at the end of the first phase transition decreases considerably, characteristic of a solid-solution domain. Taking into account the dynamic conditions of the *in situ* experiment and unavoidable inhomogeneities in the lithium content between different particles, one can suppose that the solid-solution domain upon delithiation of $Li_xCo_{0.6}Fe_{0.4}PO_4$ begins already from $x \sim 0.7$.

The difference of the unit cell volumes between the two coexisting olivine phases involved in the first phase transition is 1.7%, determined from the diffraction pattern corresponding to equal ratios of both phases. In the range $0.7 < x < 0.25$, a solid solution domain exists where the unit cell shrinks continuously. The overall change of the unit cell volume between the states at the boundary of the solid solution domain is 1.5%. For the analysis of the *in situ* diffraction patterns, starting from the $x = 0.25$ data in the charge process, a model with two coexisting olivine-like phases was applied and gave a difference in the unit cell volumes for both phases of 3%. The unit cell volume changes during lithium extraction result from a shrinkage of the *a*- and *b*-axes and a simultaneous expansion along the *c*-axis. Such an anisotropic character of unit cell evolution is observed for all mixed metallophosphates studied here (see Fig. 8).

The existence of an extended solid-solution region at intermediate charge is the most interesting feature found for $Li_xCo_{0.6}Fe_{0.4}PO_4$. Upon discharge, the re-insertion of Li into the cathode occurs *via* the same mechanism, including two two-phase regions separated by a solid-solution domain with a width of $\Delta x \sim 0.3$. The mechanism of Li insertion-extraction from $Li_xCo_{0.6}Fe_{0.4}PO_4$ is similar to the one for $LiMn_{0.6}Fe_{0.4}PO_4$. However, the solid-solution region in $LiMn_{0.6}Fe_{0.4}PO_4$ reported previously falls in the voltage range, corresponding to the electrochemical reaction Fe^{2+}/Fe^{3+}.[4,8] For

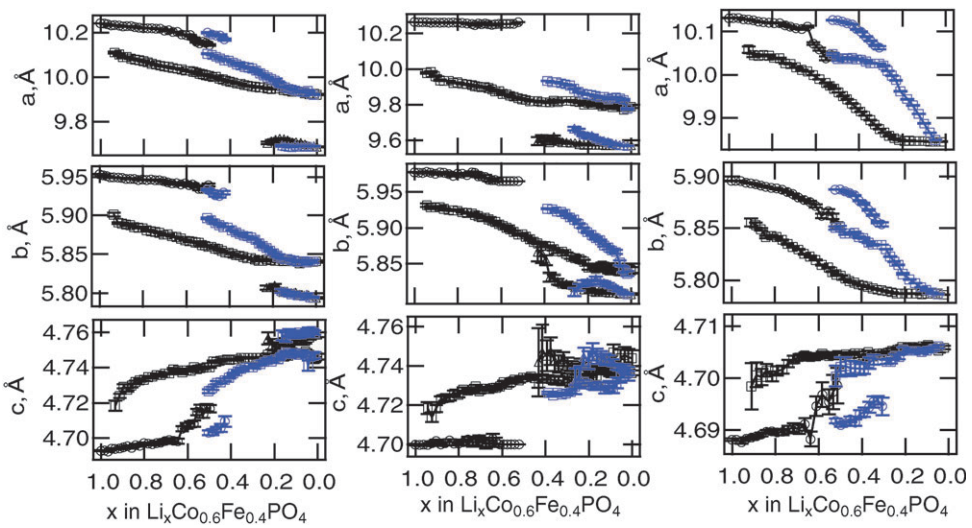

Fig. 8 Lattice parameters for the olivine-like phases, determined for all diffraction data sets. Black symbols represent charge, blue: discharge processes.

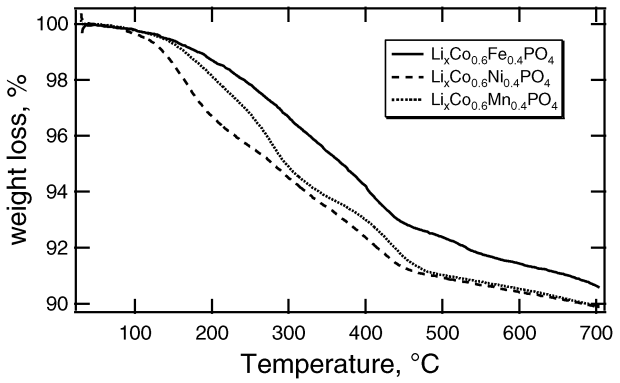

Fig. 9 Thermo-gravimetric curves of charged $LiCo_{0.6}M_{0.4}PO_4$-cathodes (M = Fe, Mn, Ni). The cells were charged up to nominal concentrations $Li_xCo_{0.6}M_{0.4}PO_4$, $x \approx 0$, as calculated from the flown charge.

$Li_xCo_{0.6}Fe_{0.4}PO_4$, the solid-solution domain is broader and includes partially a Co^{2+}/Co^{3+} electrochemical reaction.

$LiCo_{0.6}Mn_{0.4}PO_4$

The oxidation of Mn in $LiCo_{0.6}Mn_{0.4}PO_4$ during the first charge proceeds with a high overvoltage (see Fig. 1b), so that the peaks corresponding to Mn^{2+}/Mn^{3+} and Co^{2+}/Co^{3+} electrochemical processes are not well resolved in the incremental capacity plot. Nevertheless, the character of the structural changes observed during *in situ* charge of the cell is quite similar to $LiCo_{0.6}Fe_{0.4}PO_4$: a two-phase coexistence of two olivine phases in the range $1 < x < \sim 0.6$ (with a unit cell volume difference of $\sim 3.7\%$), a solid solution domain in the range $0.55 < x < 0.4$ and again a transition between two coexisting phases at the end of charge (with a difference in the unit cell volumes of $\sim 3\%$). Upon discharge, only one phase transition is observed and, therefore, the fully lithiated state $LiCo_{0.6}Mn_{0.4}PO_4$ is not reached again, probably, due to the poor kinetics involved with the Mn^{2+}/Mn^{3+} couple.

$LiCo_{0.6}Ni_{0.4}PO_4$

In contrast to the other studied metallophosphates, the charge of $LiCo_{0.6}Ni_{0.4}PO_4$ occurs *via* one phase transition region in the range $0.5 < x < 1$ (Fig. 7) only, followed by a pronounced solid-solution region up to the end of charge. The phase transition between the two olivine-like phases (unit cell volume difference is of 1.5%) is highly reversible, so that in the completely discharged state the initial phase is mainly recovered ($\sim 80\%$ w/w).

In the solid-solution region a continuous decrease of the unit cell volume during charge is visible up to $x = 0.25$ only. At high states of charge ($0.25 < x < 0$), the diffraction patterns show practically no changes. It indicates that the current in this region is due to any electrochemical reaction different from the delithiation of metallophosphate, for example, an oxidation of the electrolyte. Therefore, the oxidation of Ni in $LiCo_{0.6}Ni_{0.4}PO_4$, which should take place at higher voltages in comparison with the Co^{2+}/Co^{3+} reaction is negligible or even does not occur. This interpretation is consistent with the PITT-data (see Fig. 1c).

During discharge, a solid solution region is also well pronounced and corresponds to a $\Delta x = 0.3$, similar to the width of the solid-solution domain found for $LiCo_{0.6}Fe_{0.4}PO_4$. As for Fe and Mn-substituted compounds, the exact separation of two-phase and solid-solution domains is not unambiguously defined. Nevertheless, these solid-solution domains seem to represent a significant stage of the extraction-insertion process and may be considered as a common feature of olivine-like metallophosphates combining different electrochemically active 3d-elements in the structure.

Thermal stability of charged cathodes

As reported recently, the charged state of $LiCoPO_4$ cathodes is thermally unstable and decomposes with gases evolution at moderate heating (≥ 100 °C).[23] In charged $LiCo_{0.6}M_{0.4}PO_4$ (M = Fe, Mn, Ni) cathodes, Co^{3+} is partially replaced by other 3d elements: Fe^{3+}, Mn^{3+} or Ni^{2+} (an oxidation of Ni seems not to be reached). All three delithiated phosphates show quite similar thermal behaviour upon heating in inert atmosphere, losing ~ 6–8% of weight in the range 100–400 °C, see Fig. 9. The weight loss observed starting from 100 °C is more abrupt for the Ni-substituted cathode. These data confirm further that the presence of Co^{3+} in the olivine structure is responsible for the low thermal stability of charged 3d-metallophosphate cathodes.

Conclusions

All three metallophosphates studied here show the same character of structural changes upon electrochemical delithiation. Two-phase reactions, characteristic of olivine-type materials, are revealed for the Co^{2+}/Co^{3+} and M^{2+}/M^{3+} (M = Mn, Fe) couples in the mixed phosphates. The two two-phase regions are separated by solid-solution domains, where the unit cell volume of one olivine-type phase changes continuously. For $LiCo_{0.6}Ni_{0.4}PO_4$, only one phase transition is observed, reflecting no activity of the Ni^{2+}/Ni^{3+} couple in the investigated voltage range up to 5.25 V against Li/Li^+. Nevertheless, a solid-solution domain corresponding to 0.3 Li per formula unit is clearly observed for charge and discharge.

This study and previously reported data for $LiMn_{0.6}Fe_{0.4}PO_4$[1–3] reveals that the solid-solution domains in the olivine structure can be driven not only by particle size, but also by the intermixing of different 3d cations in the lattice. As for $LiFePO_4$,[29] the boundaries of the solid-solution domain in the investigated mixed phosphates may in principle depend on particle size as well as structural defects like non-stoichiometry or cationic disorder. This aspect may provide new approaches for the optimization of cathode materials with favorable charge–discharge characteristics.

Acknowledgements

The authors thank the Deutsche Forschungsgemeinschaft for financial support within the Priority Programme SPP 1181 "Nanoscaled Inorganic Materials by Molecular Design: New Materials for Advanced Technologies" (DFG EH183/3). Claudia Fasel (TU Darmstadt, Germany) is gratefully acknowledged for performing the thermal analyses.

References

1 A. Padhi, K. Nanjundaswamy and J. Goodenough, *J. Electrochem. Soc*., 1997, **144**, 1188.
2 A. Yamada, Y. Kudo and K.-Y. Liu, *J. Electrochem. Soc*., 2001, **148**, A747.
3 A. Yamada, Y. Takei, H. Koizumi, N. Sonoyama, R. Kanno, K. Itoh, M. Yonemura and T. Kamiyama, *Chem. Mater*., 2006, **18**, 804.
4 M. Yonemura, A. Yamada, Y. Takei, N. Sonoyama and R. Kanno, *J. Electrochem. Soc*., 2004, **151**, A1352.
5 A. Yamada, Y. Kudo and K. Liu, *J. Electrochem. Soc*., 2001, **148**, A1153.
6 J. Molenda, W. Ojczyk, K. wierczek, W. Zajak, F. Krok, J. Dygas and R.-S. Liu, *Solid State Ionics*, 2006, **177**, 2617.
7 J. Molenda, W. Ojczyk and J. Marzec, *J. Power Sources*, 2007, **174**, 689.
8 N. Bramnik, K. Bramnik, K. Nikolowski, M. Hinterstein, C. Baehtz and H. Ehrenberg, *Electrochem. Solid-State Lett*., 2005, **8**, A379.
9 C. Burba and R. Frech, *J. Power Sources*, 2007, **172**, 870.
10 X. Chang, Z. Wang, X. Li, L. Zhang, H. Guo and W. Peng, *Mater. Res. Bull*., 2005, **40**, 1513.
11 K. Zaghib, A. Mauger, F. Gendron, M. Massot and C. M. Julien, *Ionics*, 2008, **14**, 371.
12 N. Penazzi, M. Arrabito, M. Piana, S. Boloardo, S. Panero and I. Amadei, *J. Eur. Ceram. Soc*., 2004, **24**, 1381.
13 D. Wang, Z. Wang, X. Huang and L. Chen, *J. Power Sources*, 2005, **146**, 580.
14 W.-S. Yoon, K. Chung, K.-W. Nam, J. McBreen, D. Wang, X. Huang, H. Li, L. Chen and X.-Q. Yang, *J. Power Sources*, 2008, **183**, 427.
15 R. Ruffo, C. M. Mari, F. Morazzoni, F. Rosciano and R. Scotti, *Ionics*, 2007, **13**, 287.
16 S. Anandhakumar, M. Sundar and S. Selladurai, *Ionics*, 2007, **13**, 19.
17 D. Shanmukaraj, G. Wang, R. Murugan and H. Liu, *Mater. Sci. Eng., B*, 2008, **149**, 93.
18 J. Wolfenstine and J. Allen, *J. Power Sources*, 2005, **142**, 389.
19 D. Shanmukaraj and R. Murugan, *Ionics*, 2004, **10**, 88.
20 J. Wolfenstine and J. Allen, *J. Power Sources*, 2004, **136**, 150.
21 N. Bramnik, K. Nikolowski, C. Baehtz, K. Bramnik and H. Ehrenberg, *Chem. Mater*., 2007, **19**, 908.
22 H. Ehrenberg, N. N. Bramnik, A. Senyshyn and H. Fuess, *Solid State Sci*., 2009, **11**, 18.
23 N. Bramnik, K. Nikolowski, D. Trots and H. Ehrenberg, *Electrochem. Solid-State Lett*., 2008, **11**, A89.
24 K. Nikolowski, C. Baehtz, N. Bramnik and H. Ehrenberg, *J. Appl. Crystallogr*., 2005, **38**, 851.
25 M. Knapp, C. Baehtz, H. Ehrenberg and H. Fuess, *J. Synchrotron Radiat*., 2004, **11**, 328.
26 M. Knapp, V. Joco, C. Baehtz, H. H. Brecht, A. Berghaeuser, H. Ehrenberg, H. von Seggern and H. Fuess, *Nucl. Instrum. Methods Phys. Res., Sect. A*, 2004, **521**, 565.
27 A. Yamada, H. Koizumi, S. Nishimura, N. Sonoyama, R. Kanno, M. Yonemura, T. Nakamura and Y. Kobayashi, *Nat. Mater*., 2006, **5**, 357.
28 N. Meethong, H.-Y. Shadow Huang, W. Carter and Y. Chiang, *Electrochem. Solid-State Lett*., 2007, **10**, A134.
29 P. Gibot, M. Casa-Cabanas, L. Laffont, S. Levasseur, P. Carlach, S. Hamelet, J.-M. Tarascon and C. Masquelier, *Nat. Mater*., 2008, **7**, 741.